Precision of pulse-coupled networks of integrate-and-fire neurons

P H E Tiesinga[1,4] **and Terrence J Sejnowski**[1,2,3]

[1] Sloan–Swartz Center for Theoretical Neurobiology and Computational Neurobiology
Laboratory, Salk Institute, 10010 N Torrey Pines Rd, La Jolla, CA 92037, USA
[2] Howard Hughes Medical Institute, Salk Institute, La Jolla, CA 92037, USA
[3] Department of Biology, University of California—San Diego, La Jolla, CA 92093, USA

E-mail: tiesinga@salk.edu

Abstract
Some sensory tasks in the nervous system require highly precise spike trains
to be generated in the presence of intrinsic neuronal noise. Collective
enhancement of precision (CEP) can occur when spike trains of many neurons
are pooled together into a more precise population discharge. We study CEP in
a network of N model neurons connected by recurrent excitation. Each neuron
is driven by a periodic inhibitory spike train with independent jitter in the spike
arrival time. The network discharge is characterized by σ_W, the dispersion in
the spike times within one cycle, and σ_B, the jitter in the network-averaged
spike time between cycles. In an uncoupled network $\sigma_B \sim 1/\sqrt{N}$ and σ_W is
independent of N. In a strongly coupled network $\sigma_B \sim 1/\sqrt{\log N}$ and σ_W
is close to zero. At intermediate coupling strengths, σ_W is reduced, while σ_B
remains close to its uncoupled value. The population discharge then has optimal
biophysical properties compared with the uncoupled network.

1. Introduction

The nervous system is capable of producing extremely precise periodic electrical discharges
necessary for sensory tasks such as electroreception. As an example of this phenomenal
precision, the coefficient of variation (CV)—the standard deviation of the period divided by
the mean period—is $\sim 10^{-4}$ for the electric organ discharge generated by the pacemaker nucleus
in weakly electric fish [1]. This discharge is produced by a network consisting of 100–150
neurons sparsely connected by electric gap junctions and possibly by chemical synapses.
There are two types of neuron in the network, pacemaker cells and relay cells. It is not
known how networks of neurons can generate highly precise spike trains in the presence of
intrinsic noise [2, 3]. One possible strategy is to pool the discharge of many neurons into a
more precise population discharge [4, 5]. This would reduce the jitter in the average spike

---

[4] To whom correspondence should be addressed.

time of N uncoupled neurons in a given oscillation cycle to $1/\sqrt{N}$ times that of the jitter of a single neuron. Hence the precision, defined as the inverse of the jitter in average spike time, is improved by a factor of $\sqrt{N}$. The typical spike-timing jitter in the spike train of a single neuron in the neocortex is about 1 ms [7]. The jitter for an isolated pacemaker or relay cell in the pacemaker nucleus is not known. Hence, based on neocortical physiology, the jitter in the pacemaker nucleus could be reduced to approximately $1 \text{ ms}/\sqrt{100} = 100 \mu s$. However, jitter as small as 0.1–1 μs was obtained in experiments [1]. There are two possible reasons for this discrepancy: the pacemaker and relay cells have biophysical specializations in order to lower the level of intrinsic noise, or the high precision is an emergent property of the coupled network. The fundamental question is thus whether one can improve on the $\sqrt{N}$ result by using a network of coupled neurons [6].

Here we study a network of neurons coupled via recurrent excitation, with each neuron driven by a periodic inhibitory spike train with independent jitter (with variance σ_ϕ^2) in the spike arrival time. The key quantities characterizing the network discharge are σ_W, the dispersion in the spike times within one cycle; and σ_B, the jitter in the network-averaged spike time between cycles. Thus, the precision for the network is the inverse of σ_B. The network discharge can be entrained to the periodic drive. For instance, during 1:1 entrainment each neuron emits one spike for each arriving inhibitory pulse. We address the following questions. How does the output precision depend on the input jitter σ_ϕ? How does it depend on the network size N? Can excitatory coupling improve the precision compared with an uncoupled network?

Our main results are as follows. Optimal precision is attained during entrainment, where the output jitter depends linearly on the input jitter. The improvement in optimal precision for an uncoupled network goes as $\sqrt{N}$ as a result of the law of large numbers [8], and is always higher compared with $\sqrt{\log N}$ for the strongly coupled network. The $\sqrt{\log N}$ can be understood intuitively as follows. In the strongly coupled network all neurons spike at the same time, since the first neuron to spike immediately recruits all other neurons in the network. Hence, the jitter in the network spike time, σ_B, is determined by the variance, $\sqrt{\log N}$, of the distribution of the earliest spike time among N independent, identically distributed spike times. At intermediate coupling strength the precision, $1/\sigma_B$, can still improve as $\sqrt{N}$, while the dispersion σ_W in the spike times within one cycle is reduced compared with the uncoupled case.

We first present an efficient algorithm for the simulation of large pulse-coupled networks, and introduce the statistical measures that we calculate. The precision of an uncoupled and a strongly coupled network was derived analytically, while the precision for intermediate coupling strengths was determined using numerical simulations. Finally we discuss the relative benefits of a coupled compared with an uncoupled network.

2. Methods

2.1. Dynamical equations

We study the dynamics of an integrate-and-fire (IAF) model neuron driven by a periodic inhibitory spike train with period $T = 1$. The dynamics is given by

$$\frac{dV_n}{dt} = -V_n + I_0 - p \sum_m \delta(t - \phi - \Delta\phi_m^n - mT) + E(t), \tag{1}$$

where V_n is the membrane potential of the nth neuron, $n = 1, \ldots, N$, N is the number of neurons, I_0 the driving current and p the strength of the inhibitory pulse. The inhibitory pulses arrive in cycle m at relative phase ϕ with some jitter $\Delta\phi_m^n$, and $m = 1, 2, \ldots$. The jitter is

independent for each neuron, uncorrelated between cycles, and is normally distributed with mean zero and variance σ_ϕ^2. The neurons are coupled all-to-all with instantaneous excitatory synapses, yielding an excitatory current,

$$E(t) = \frac{g}{N} \sum_{n,i} \delta(t - t_i^n),$$

with total coupling strength g, and the sum is over all spike times t_i^n. Here t_i^n is the ith spike time of the nth neuron. When the voltage V_n crosses 1 a spike is emitted, and the voltage is reset to V_0. Here we take $V_0 = 0$.

2.2. Spike time map for a single neuron on the entrainment step

During 1:1 entrainment the neuron produces one spike on each cycle; the spike index i is then equal to the cycle index m. In this subsection we will suppress the neuron index n and use m instead of i. We derive a map for a single neuron on the 1:1 entrainment step that predicts the new spike time t_{m+1} in the next cycle $m + 1$ given the spike time t_m in the previous cycle m. This map is studied in section 3. Equation (1) is integrated with $g = 0$ from the last spike at $t_m = mT + \psi_m$ to the next spike at $t_{m+1} = (m + 1)T + \psi_{m+1}$, where $\psi_m = \mathrm{mod}(t_m, T)$ is the spike phase. The membrane potential after the arrival of the first inhibitory pulse at $mT + \phi + \Delta\phi_m$ is

$$V' = e^{-(\phi + \Delta\phi_m - \psi_m)}(V_0 - I_0) + I_0 - p, \tag{2}$$

and the voltage at later time $t > mT + \phi + \Delta\phi_m$ is

$$V(t) = e^{-(t - mT - \phi - \Delta\phi_m)}\left[V' - I_0\right] + I_0. \tag{3}$$

The neuron spikes when it reaches threshold, $V(t) = 1$, yielding the following map in terms of the spike phase, ψ_m:

$$\begin{aligned} \psi_{m+1} &= \ln\left[a(V_0)e^{\psi_m} + be^{\Delta\phi_m}\right] - T \\ &= \psi_m + \ln\left[a(V_0) + be^{\Delta\phi_m - \psi_m}\right] - T \end{aligned} \tag{4}$$

here we used

$$a(V_0) = \frac{I_0 - V_0}{I_0 - 1}, \tag{5}$$

$$b = \frac{p\exp(\phi)}{I_0 - 1}. \tag{6}$$

In the following expressions we suppress the dependence of a on V_0. In the absence of input jitter, $\sigma_\phi = 0$, the fixed-point phase ψ is found by substituting $\psi_{n+1} = \psi_n = \psi$ in equation (4), yielding a period $T = \ln(a + be^{-\psi})$. To simplify the analytical calculation it is useful to choose ϕ for each I_0 such that $\psi = 0$, yielding $T = \ln(a + b)$. In this way the inhibitory pulse in cycle m will be guaranteed to happen after the spike ψ_m. However, in the numerical simulations (described below) we keep ϕ fixed and ψ is allowed to vary with I_0.

2.3. Network simulations

We simulate the network dynamics of equation (1) as follows. The state of the network is described by the set of membrane potentials $\{V_1, \ldots, V_N\}$ at time t_1. If the current drive to each neuron is the same, the one with the highest voltage, V_n, would spike first. Note that in a synchronized network there may multiple neurons with a membrane potential equal to V_n. We estimate the next spike time as

$$t_2 = t_1 + \ln\frac{I_0 - V_n}{I_0 - 1}. \tag{7}$$

Here we assume that $I_0 > 0$ and define t_2 to be equal to t_1 when $V_n = 1$. We then find all the inhibitory pulses that arrive between t_1 and t_2 and update the membrane potential to the time immediately after pulse arrival (at t_p^n for the nth neuron):

$$V_n' = e^{-(t_p^n - t_1)}(V_n - I_0) + I_0 - p. \tag{8}$$

There may be multiple pulses per neuron, but for simplicity the above notation does not reflect this. Then, all of the neurons are updated to t_2: neurons that received inhibitory pulses,

$$V_n'' = e^{-(t_2 - t_p^n)}(V_n' - I_0) + I_0, \tag{9}$$

and the ones that did not,

$$V_n'' = e^{-(t_2 - t_1)}(V_n - I_0) + I_0. \tag{10}$$

We then determine which neurons actually crossed the threshold, $V_i'' > 1$, reset their voltage to zero, and emit an excitatory pulse to all neurons. We again check which neurons reached threshold, then their membrane potential is reset to 1 so they would spike immediately, $t_2 = t_1$, in the next iteration of equation (7). This algorithm leads to a large speed-up compared with direct integration using the Runge–Kutta algorithm [9]. In addition, it predicts to machine precision the spike time, whereas for direct integration the spike time is a multiple of the integration time step (see also [10]).

2.4. Calculated quantities

From the set of spike times t_i^n we compute the phases $\psi_i^n \equiv \mathrm{mod}(t_i^n, T)$, where t_i^n is the ith spike time of the nth neuron. The temporal and network average of the spike-time jitter is

$$\sigma_\psi^2 = \frac{1}{NM} \sum_{n=1}^{N} \sum_{m=1}^{M} \sum_{i(n,m)} (\psi_i^n)^2 - \mu^2, \tag{11}$$

where the mean phase is

$$\mu = \frac{1}{NM} \sum_{n=1}^{N} \sum_{m=1}^{M} \sum_{i(n,m)} \psi_i^n. \tag{12}$$

Here N is the number of neurons in the network, and M the number of cycles in the simulation run after a transient, $\sum_n$ is the sum over all neurons, $\sum_m$ is the sum over all cycles and $\sum_{i(n,m)}$ is the sum over all spikes i of neuron n that occurred on cycle m *normalized* by the number of these spikes. (Note that on some cycles neuron n may not produce any spikes, whereas during 1:1 entrainment we have the identity $i(n, m) = m$.) The jitter σ_ψ is the sum of two contributions,

$$\sigma_\psi^2 = \sigma_W^2 + \sigma_B^2. \tag{13}$$
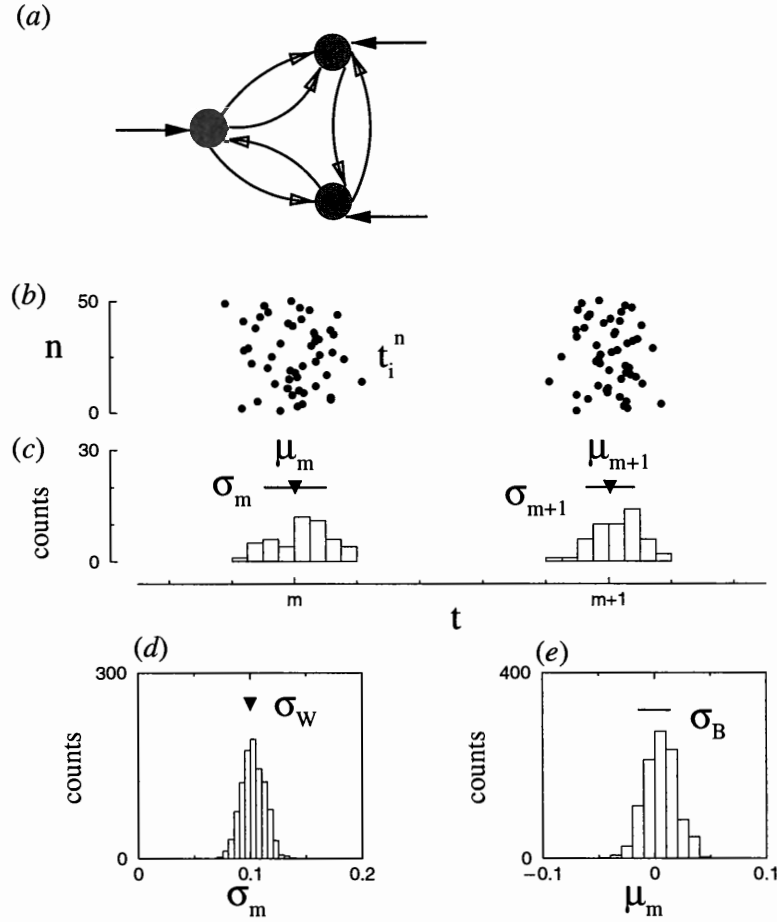
Here we used the following definitions:

$$\sigma_W^2 = \frac{1}{M} \sum_{m=1}^{M} \sigma_m^2, \tag{14}$$

$$\sigma_B^2 = \frac{1}{M} \sum_{m=1}^{M} \mu_m^2 - \mu^2, \tag{15}$$

and

$$\mu_m = \frac{1}{N} \sum_{n=1}^{N} \sum_{i(n,m)} \psi_i^n, \tag{16}$$

$$\sigma_m^2 = \frac{1}{N} \sum_{n=1}^{N} \sum_{i(n,m)} (\psi_i^n)^2 - \mu_m^2. \tag{17}$$

Figure 1. Illustration showing the calculation of σ_B and σ_W. (a) Schematic diagram of the network model consisting of IAF neurons coupled all-to-all with excitatory synapses (open arrows) and driven by inhibitory inputs (filled arrows). (b) Rasterplot for cycles m and $m + 1$; the ith spike time of the nth neuron is shown as a filled circle with its index n as y-ordinate and its spike time t_i^n as x-ordinate. (c) Histogram of spike times; μ_m (filled triangle) is the average, and σ_m (solid line) is the standard deviation of all the spikes during cycle m. (d) Histogram of σ_m; σ_W (solid triangle) is the average of this distribution. (e) Histogram of μ_m; σ_B (solid line) is the standard deviation of this distribution.

The calculation of σ_W and σ_B is illustrated in figure 1. σ_W measures the jitter around the average phase in a particular cycle. If the network is fully synchronized—all the neurons fire approximately at the same time in each cycle—σ_W will approach zero. In contrast, σ_B measures the variation of the average spike phase μ_m in a particular cycle. It varies as $\sigma_B \sim 1/\sqrt{N}$ for uncoupled neurons (equation (26)). The precision of the population discharge is given by $1/\sigma_B \sim \sqrt{N}$, and increases with increasing N. The definition of the phase has a discontinuity: once a phase changes from say 0.99 to 1.01 it is mapped to 0.01. This means that a unimodal distribution of phases centred near 1 would be mapped to two peaks, leading to a higher variance. To prevent this the pulses are applied at $\phi = 0.8$.
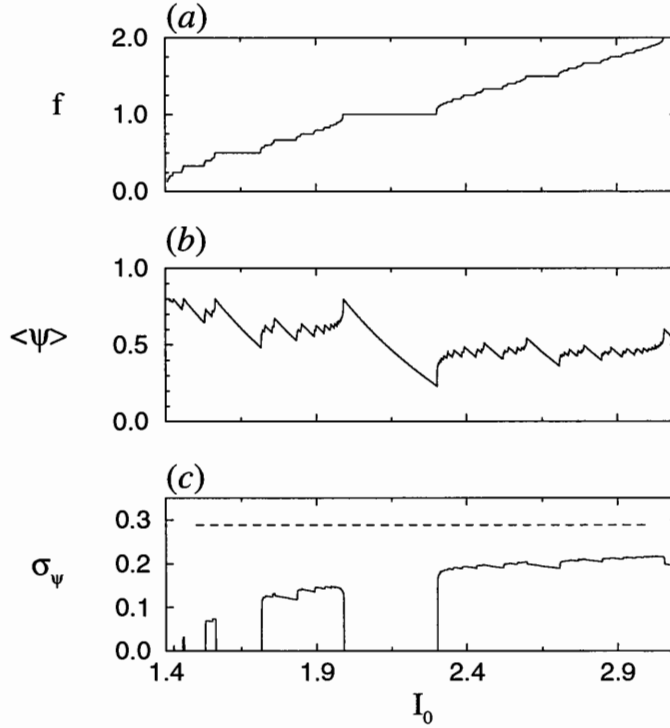
Figure 2. Phase locking of an IAF neuron to an inhibitory pulse train. (a) The firing rate f, (b) the average spike phase $\langle \psi \rangle$ and (c) the output jitter σ_ψ as a function of current I_0. The dashed line in (c) indicates the standard deviation, $1/\sqrt{12}$, when the phases are uniformly distributed between zero and one. We use the following parameter values: $p = 0.7$; $\sigma_\phi = 0$; $\phi = 0.8$. The averages are over 10×10^3 cycles, after discarding the initial 200 cycles.

3. Results

3.1. Single neuron with zero input jitter

The firing rate versus current (f–I) characteristic of a current-driven IAF neuron is

$$f = \frac{1}{\ln \frac{I_0 - V_0}{I_0 - 1}}. \tag{18}$$

The neuron does not spike for currents $I_0 < 1$. For currents $I_0 > 1$ the firing rate increases smoothly with increasing current. Here we consider an IAF neuron driven by a periodic inhibitory pulse train with $I_0 > 1$. The emitted spike train can then be entrained, or phase locked, to the input. This leads to steps in the f–I characteristic (figure 2(a)). On a step the firing rate is constant for a range of current values, and equal to a fraction $\frac{n}{m}$ of the driving frequency (here n and m should not be confused with the neuron and cycle index, respectively). The neuron emits n spikes in m cycles of the drive. We now focus on the 1:1 ($n = 1, m = 1$) step located between $I_0 = 2.0$ and 2.3 for $p = 0.7$. The pulse arrives each cycle at phase $\phi = 0.8$, and the neuron spikes each cycle at phase ψ. At the left-hand side of the step the neuron spikes shortly before the arrival of the next inhibitory pulse. For increasing current the neuron spikes earlier, and ψ decreases (figure 2(b)).

The precision of a single neuron is the inverse of the standard deviation σ_ψ of the spike phase. A larger σ_ψ thus means a lower precision. In figure 2(c) we plot σ_ψ versus current. It is zero on the 1:1 and 1:m steps and it is nonzero outside these steps.

3.2. Single neuron with input jitter

Now consider the case when the inhibitory pulses arrive with a temporal jitter σ_ϕ. Their arrival phase ϕ_m is independent in each cycle, and distributed according to Gaussian probability distribution with mean ϕ, and variance σ_ϕ^2. In this subsection we again have suppressed the neuron index n. The input jitter introduces jitter in the output spike train on the 1:1 step. The spike time in the mth cycle is $t_m = mT + \psi_m$. The spike phase ψ_m jitters around its stationary value ψ according to equation (4),

$$\psi_{m+1} = \psi_m + \ln\left[a(V_0) + b e^{\Delta\phi_m - \psi_m}\right] - T. \tag{19}$$

Note that a and b were defined in equations (5) and (6), $\Delta\phi_m$ is the jitter in the pulse arrival time.

Given the distribution of the input jitter,

$$P_{\Delta\phi}(\Delta\phi_m) = \frac{1}{\sqrt{2\pi\sigma_\phi^2}} \exp\left(-\frac{\Delta\phi_m^2}{2\sigma_\phi^2}\right), \tag{20}$$

and the value of the previous phase ψ_m, the distribution of the next phase ψ_{m+1} is

$$Q(\psi_{m+1}|\psi_m) = J(\psi_{m+1}) P_{\Delta\phi}\left(\ln\frac{e^{T+\psi_{m+1}} - a e^{\psi_m}}{b}\right). \tag{21}$$

Here we used

$$J(\psi_{m+1}) = \frac{\mathrm{d}\Delta\phi_m}{\mathrm{d}\psi_{m+1}} = \frac{e^{T+\psi_{m+1}}}{e^{T+\psi_{m+1}} - a e^{\psi_m}}.$$

Equation (21) is obtained by inverting equation (19) to express $\Delta\phi_m$ as function of ψ_{m+1}, and then multiplying the $P_{\Delta\phi}$ by the Jacobian J. The distribution for ψ_m in cycle m is obtained by iterating the following equation starting from a distribution P_0 for the starting phase difference ψ_0:

$$P_{m+1}(\psi_{m+1}) = \int \mathrm{d}\psi_m \, Q(\psi_{m+1}|\psi_m) P_m(\psi_m).$$

In numerical simulations the distribution $P_m(\psi_m)$ converged to a stationary distribution P_s. We have not established whether this holds for all parameters and initial conditions. The stationary distribution is a solution of

$$P_s(t) = \int \mathrm{d}s \, Q(t|s) P_s(s). \tag{22}$$

Equation (22) turns into a matrix equation $P_j = \sum_i Q_{ij} P_j$ when ψ takes discrete values labelled by the indices i and j. The stationary distribution then corresponds to the eigenvector at eigenvalue $\lambda = 1$. We numerically determined the stationary distribution using Matlab (MathWorks). For small jitter, $\sigma_\phi \ll T$, one can instead linearize equation (19) in terms of the small deviations $\Delta\psi_m = \psi_m - \psi$. To simplify, without loss of generality, we have chosen ϕ such that $\psi = 0$ (see section 2), yielding

$$\Delta\psi_{m+1} = \frac{a}{a+b}\Delta\psi_m + \frac{b}{a+b}\Delta\phi_m. \tag{23}$$
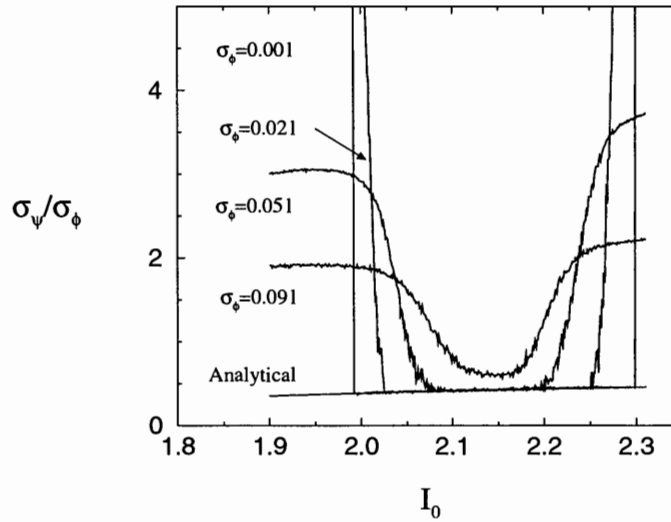
Figure 3. Output spike jitter σ_ψ normalized by the input jitter σ_ϕ as a function of current on the 1:1 entrainment step for $\sigma_\phi = 0.001, 0.021, 0.051$ and 0.091 as labelled. The solid curve is the analytical curve from of equation (24). We use $p = 0.7$ and $\phi = 0.8$. The averages are over 50×10^3 cycles, after discarding the initial 2×10^3 cycles.

After an initial transient the distribution of $\Delta \psi_n$ converges to a stationary distribution. Hence the moments of the distribution in consecutive cycles are the same, $\langle \Delta \psi_{m+1}^2 \rangle = \langle \Delta \psi_m^2 \rangle$. Together with equation (23) this yields the following expression for the output jitter as a function of the input jitter:

$$\sigma_\psi^2 = \langle \Delta \psi_m^2 \rangle = \frac{\langle \Delta \phi_m^2 \rangle}{1 + 2a(0)/b} \equiv c_0^2 \sigma_\phi^2. \tag{24}$$

The above equation defines the proportionality constant c_0. The average and variances of the numerically determined distribution P_s are in excellent agreement with equation (24) for $\sigma_\phi < 0.05$ (not shown).

We also performed direct simulations based on equation (1) for different values of σ_ϕ (with parameters values $N = 1$ and $g = 0$). We plot in figure 3 the output jitter as a function of current on the 1:1 step, together with the results of equation (24). The numerical simulations only agree with the analytical expression for current values in the middle of the step. The width of this region decreases with increasing input jitter, and disappears for $\sigma_\phi > 0.05$. In order to understand why the analytic expression fails near the edges of the step we examine how the phase locking on the 1:1 step becomes unstable for low and high currents. For low currents, near the left-hand edge of the step, the neuron spikes just before the arrival of the next inhibitory pulse. If the current were reduced even more, the pulse would arrive before the spike is emitted. This would delay the spike even further into the next cycle. Therefore we have a cycle without any spikes: the neuron has skipped a cycle. Skipping destabilizes the phase locking. Due to jitter the inhibitory pulse can arrive before the neuron would spike, even on the entrainment step. The neuron will then spike in the next cycle, but at a phase far from its average value ψ. It takes a few cycles to return to its stationary value. The skipping leads to extra output jitter that is not accounted for in our analytical treatment.

The time series of the spike phases and the resulting return map is shown in figure 4. The time series for $I_0 = 2.15$ (the middle of the step) consists of small deviations around the
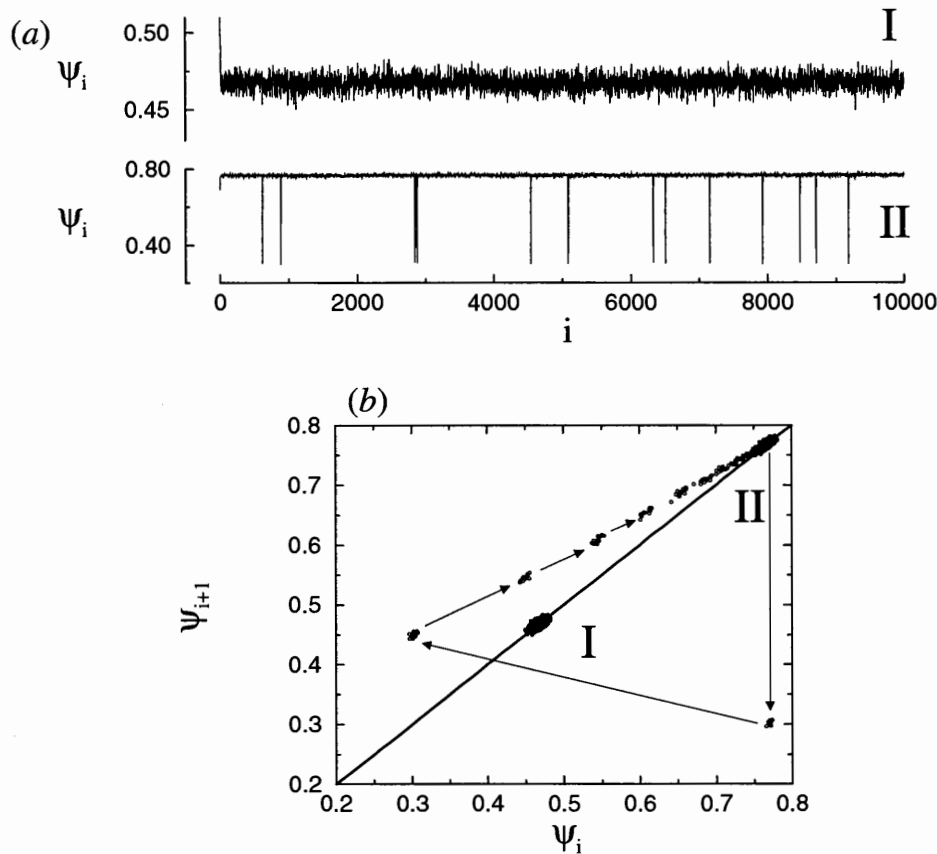
Figure 4. Spike skipping near the right-hand edge of the 1:1 entrainment step. (a) The spike phase versus index i; (b) the return map (the phase ψ_{i+1} versus the phase ψ_i). The solid line is $\psi_{i+1} = \psi_i$. The location of the fixed point of the map is given by its intersection with the solid line. The arrows indicate the temporal progression of the dynamics after a skip. Here (I) $I_0 = 2.15$ and (II) $I_0 = 2.0028$ with $p = 0.7$, $\phi = 0.8$ and $\sigma_\phi = 0.01$.

average $\psi = 0.47$. In the return map we plot the phase ψ_{i+1} versus the previous phase ψ_i: it consists of a compact cluster of dots. In contrast, the time series for $I_0 = 2.0028$ ($\psi = 0.77$) is characterized by infrequent large deviations when the neuron skips a cycle. During skipping the phase jumps from $\psi_i \approx 0.77$ to 0.3, then it returns to 0.77 over the next few cycles. The return map now consists of multiple clusters of points.

On the right-hand edge of the current step the neuron spikes long before the next inhibitory pulse arrives. For an even higher value of the current the neuron can spike again before the pulse arrives. In that case there are two spikes in one cycle, and the next spike will happen at a phase far from the fixed-point phase. In this way the phase locking becomes unstable. In the presence of jitter the inhibitory pulse can arrive at a later time, and therefore the neuron can spike twice in one cycle even on the entrainment step. This leads to increased output jitter in an analogous fashion to skipping.

To summarize, the output jitter attains its minimum on the entrainment step. There it is linearly proportional to the input jitter. The width of the linear region decreases for increasing input jitter.

3.3. Uncoupled network

For the uncoupled network the average spike time μ_m is the sum of N independent variables ψ_m^n, each satisfying equation (19), and with standard deviation σ_ψ. (The phase distribution is not Gaussian, though for small σ_ϕ it is a good approximation.) Hence, for large N, using the law of large numbers [8], the standard deviation of μ_m will approach

$$\sigma_B = \frac{\sigma_\psi}{\sqrt{N}}, \tag{25}$$

and since the distribution of all the phases is the same as the distribution of each individual phase, $\sigma_W \approx \sigma_\psi$.

On the entrainment step $\sigma_\psi \approx c_0 \sigma_\phi$, hence

$$\sigma_B \approx \frac{c_0 \sigma_\phi}{\sqrt{N}}. \tag{26}$$

These results are confirmed using direct simulation of the ensemble of neurons in the next subsection.

3.4. Strongly coupled network

We now discuss the dynamics of a network of IAF neurons coupled all-to-all via excitatory pulses. Previously it was shown that excitatory coupling can lead to synchronization [11–14]. Here, each neuron in addition receives the same periodic inhibitory pulse train. However, the jitter in the pulse arrival time is uncorrelated between different neurons. This network converges for strong enough coupling to a synchronized state in which all neurons fire at the same time. Just after the neurons fire, they each receive N excitatory pulses of strength g/N. This instantaneously increases the membrane potential from its reset value 0 to g. In the time interval just after the last spike and just before the next spike there are no other excitatory pulses, hence the dynamics of each network neuron is reduced to equation (4), with initial condition $V_0 = g$. In the absence of input jitter all neurons have identical dynamics and thus the network spike times are also given by equation (4). Once again there are phase-locked solutions, including the 1:1 entrainment step. The position of the step is shifted to lower current values due to the excitatory coupling. However, because of the coupling the effects of the input jitter are different from before. The first neuron to spike will emit pulses to other neurons. As a result they will all spike earlier. If the coupling is strong enough and the voltage distribution is sharp enough, the first spike will make all other neurons spike immediately afterwards. The network spike times are thus given by the earliest spike time of an ensemble of noisy uncoupled neurons.

In equation (4), ψ_{m+1} increases as a function of $\Delta\phi_m$, therefore the earlier the inhibitory pulse arrives, the sooner the neuron spikes. Since in the synchronized state all neurons have the same membrane potential, the neuron that receives the earliest inhibitory pulse will spike first. The distribution of earliest pulse times is equal to the distribution $P_{\min}(\Delta\phi_m^{\min})$ of the minimum $\Delta\phi_m^{\min}$ of N randomly drawn deviates $\Delta\phi_m^n$ from a Gaussian probability distribution. The analytical expression for $P_{\min}$ and the asymptotic values of its first and second moment are given in the appendix. The dynamics of the synchronized spike phase of the whole network is thus given by equation (4) driven by a pulse train with jitter $\Delta\phi_m^{\min}$. The distribution $P_{\min}$ is different from $P_{\Delta\phi}$ in two ways. First, the average $\langle\Delta\phi_m^{\min}\rangle$ is nonzero. The expected value for the minimum of N deviates with average zero is negative, asymptotically $\langle\Delta\phi_m^{\min}\rangle \sim -\sqrt{\log N}$. Second, the distribution is more sharply peaked; the standard deviation scales asymptotically as $\sigma_{\text{eff}} \sim \sigma_\phi/\sqrt{\log N}$. The distribution is asymmetric: the tail on the left-hand side is longer than the one on the right-hand side. We can now repeat the analysis done on equation (19) with
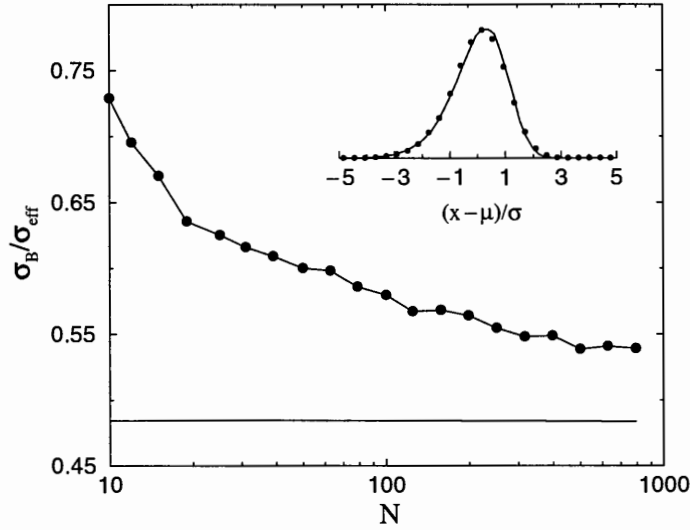
Figure 5. Output spike jitter σ_B normalized by σ_{eff} (filled circles) and the analytical result equation (24) (solid curve). In the inset we plot the distribution of μ_m (circles) and of $\Delta\phi_m^{\min}$ (solid curve). The x-ordinate is scaled so both distributions have zero mean and unit variance. Here $g = 0.4$, $p = 0.7$, $\phi = 0.8$ and $\sigma_\phi = 0.01$. Averages are over 80×10^3 cycles, after discarding the initial 200 cycles.

input jitter according to the new distribution $P_{\min}$. The spike times generated by equation (19) are now the spike times of the network, instead of those of a single neuron. There was good agreement between results obtained by discretizing equation (22) and those obtained by linearization of equation (19), $\sigma_\psi = c_g \sigma_\phi$, $c_g = \frac{1}{1+2a(V_0=g)/b}$ (not shown). Since the earliest pulse $\Delta\phi_m^{\min}$ arrives on average at phase $\phi' = \phi + \langle\Delta\phi_m^{\min}\rangle$ we use ϕ' instead of ϕ in equation (6) for b. We have also determined using simulations of the full network the distribution of $\Delta\phi_m^{\min}$ and the average spike phase μ_m (see equation (16)). We rescaled them by their average μ and variance σ: $y = (x-\mu)/\sigma$ with $x = \Delta\phi_m^{\min}$ (or μ_m) and plotted them both in figure 5. The two distributions have approximately the same shape. The ratio $\sigma_\psi/\sigma_{\text{eff}}$ obtained from simulations comes closer to the theoretical value c_g as N increases. We did not establish whether $\sigma_\psi/\sigma_{\text{eff}}$ would converge to c_g for even larger N. The analytical result only yields qualitatively correct results for the network sizes studied here and it should be interpreted as a lower bound for σ_ψ.

We now describe the results of the simulations of the full network in more detail. In figure 6 we compare the behaviour of the precision as a function of N for two different current values, $I_0 = 1.77$, close to the left-hand edge of the step, and $I_0 = 1.88$ in the middle of the step. In the middle of the step σ_B only decreases very slowly with increasing N. It provides the largest part of σ_ψ. The jitter σ_W starts out at values close to zero for a small network with $N = 10$. This means that the network is almost fully synchronized. However σ_W increases with system size, and levels off for $N > 100$. For larger networks the effect of a single excitatory pulse, g/N, is not strong enough to immediately bring all other neurons to threshold, leading to dispersion in the spike times within a cycle. The average arrival phase of the first pulse is $\phi + \langle\Delta\phi_m^{\min}\rangle$ (the average is over the cycles m). The earliest inhibitory pulse moves to an earlier phase for increasing N, hence the spike phase μ also moves to earlier times (figure 6(f)).

Next, consider the edge of the step. The jitter σ_B decreases quickly with increasing N (figure 6(a)). In this case the largest contribution to σ_ψ is given by σ_W (figure 6(c)).
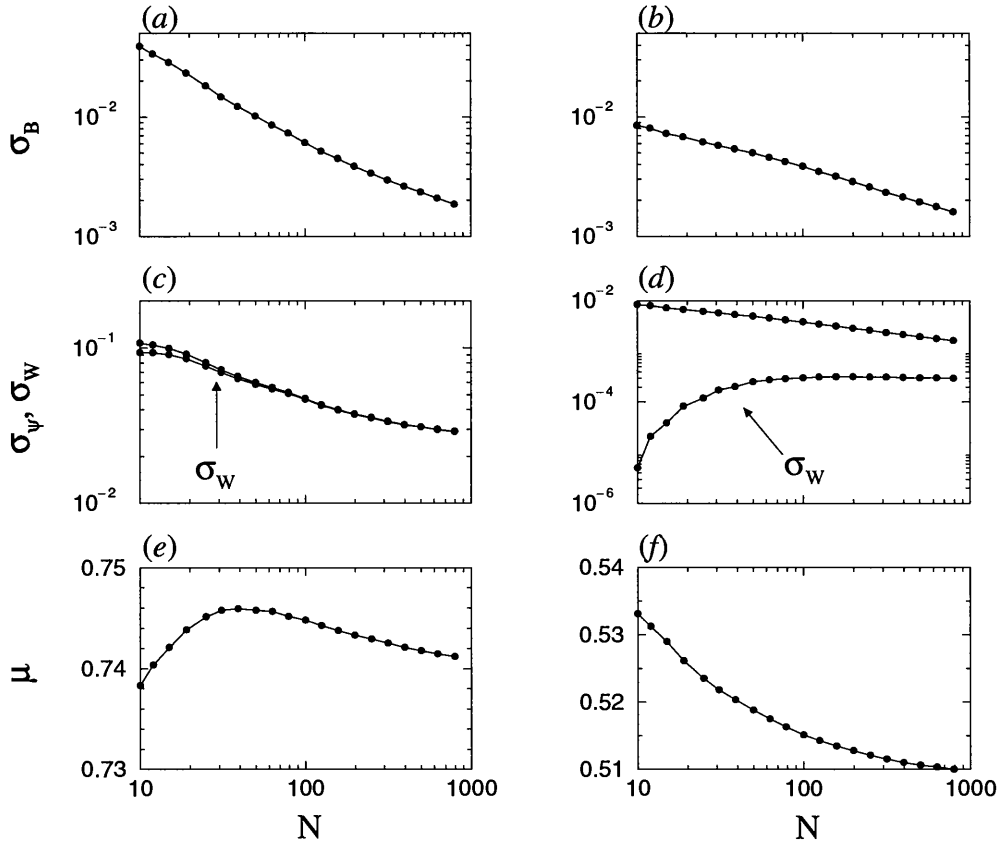
Figure 6. Precision as a function of network size, N. Plots of (a), (b) σ_B, (c), (d) σ_W and σ_ψ and (e), (f) μ versus N (definitions are given in the section 2). Here (a), (c), (e) $I_0 = 1.77$, and (b), (d), (f) $I_0 = 1.88$. The other parameters are $g = 0.4$, $p = 0.7$, $\phi = 0.8$ and $\sigma_\phi = 0.01$. Averages are over 40×10^3 cycles, after discarding the initial 200 cycles.

The decrease in σ_ψ is therefore due to an increase in synchronization as measured by σ_W. Interestingly, μ depends nonmonotonically on N (figure 6(e)). To understand this in more detail we study the time trace of the phase of one individual neuron in the network for $N = 10$ and 79 (figures 7(a) and (b)). The time series consists of small deviations from the average, interspersed with large deviations due to skipping. The frequency of skipping depends on network size: for $N = 10$ it occurs more frequently compared with $N = 79$. Skipping increases the value of σ_W and σ_B. We have also plotted the probability distribution of the spike phase, with the large deviations excluded (figures 7(c), (d)). Two features change when increasing N. The mean of the distribution moves away from $\phi = 0.8$, and the distribution becomes sharper. These two changes make it harder for skipping to occur in larger networks. The increase in precision with N near the edge is therefore partly due to the suppression of skipping, and partly due to the reduced jitter in $\Delta\phi_m^{\min}$.

We now investigate how the increase in precision of a strongly coupled network compares to that in uncoupled networks. There are two questions to be addressed. Firstly, how does the precision increase with N compared with the initial precision at a small network size (here $N = 10$)? We therefore plot $\sigma_B(N)/\sigma_B(10)$ versus N in figures 8(a) and (b). In the middle
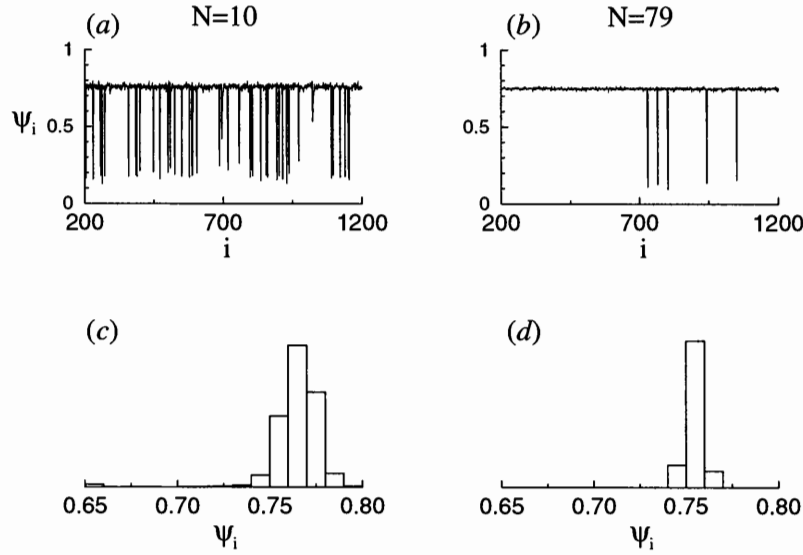
Figure 7. The spike phase and its probability distribution. Plots of (a), (b) the spike phase ψ_i versus index i, and (c), (d) its distribution with large deviations ($\psi_i < 0.6$) excluded. Here $N = 10$ (a), (c) and $N = 79$ (b), (d), and $g = 0.4$, $p = 0.7$, $\phi = 0.8$, $\sigma_\phi = 0.01$.

part of the step the precision of the uncoupled network increases faster with N than in the coupled network (figure 8(a)). However, near the edge the coupled network performs better than the uncoupled network (figure 8(b)). The second question is how the output jitter σ_B varies with N, compared with the input jitter σ_ϕ. In figures 8(c) and (d) we therefore plot σ_B/σ_ϕ. We find that the uncoupled network always has a higher precision compared with a strongly coupled network. Near the edge of the step the coupled network performs almost an order of magnitude worse compared with the uncoupled network.

3.5. Precision for intermediate strength of the coupling

In figure 9 we show the crossover in the precision from its value in the uncoupled network to its value in the strongly coupled network. The spike phase shifts to earlier times in the cycle when g is increased at a fixed current. To allow for an unbiased comparison we decrease the current as a function of g to keep the fixed-point spike phase ψ constant. We first discuss the results for $\sigma_\phi = 0.005$. The roman numerals refer to the labels in figure 9. (I) σ_W and σ_B remain constant up to $g \sim 10^{-4}$. (II) For values between $g \sim 10^{-4}$ and $g \sim 10^{-2}$, σ_W decreases sharply, but σ_B remains approximately equal to its $g = 0$ value. (III) For $g > 10^{-2}$, the decrease in σ_W is reduced, but σ_B increases. At $g \sim 1$, the strongly coupled limit is reached: σ_W is close to zero.

The onset of the decrease in σ_W (II) shifts to higher coupling strengths for increasing σ_ϕ. The increase in σ_B (III) is still coupled to the levelling off of the decrease in σ_W. However, at higher coupling strength (IV) the phase locking becomes unstable: both σ_W and σ_B increase.

To summarize, at intermediate coupling strengths σ_B stays close to its optimal $g = 0$ value, but σ_W can be reduced by increasing g. The quantities $\sigma_B \sqrt{N}/\sigma_\phi$ and σ_W/σ_ϕ saturate as a function of N for $N > 79$ (not shown).
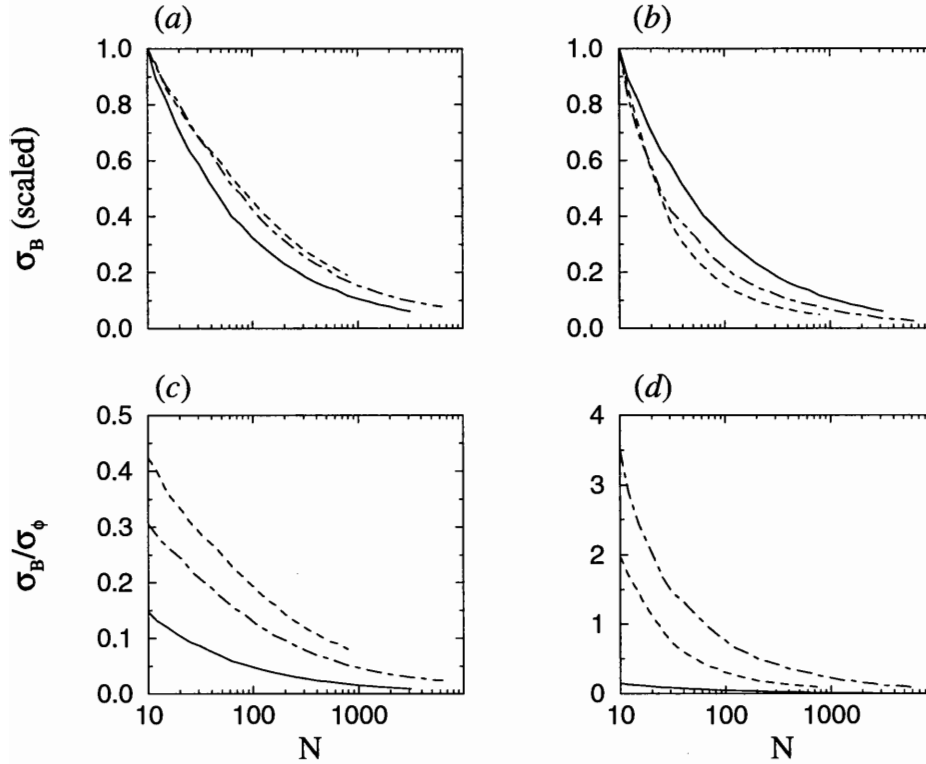
Figure 8. Scaling of precision with network size. Plots of (a), (b) $\sigma_B(N)/\sigma_B(10)$ and (c), (d) $\sigma_B(N)/\sigma_\phi$ versus network size N. The reference curve (solid curve) for an uncoupled network at $I_0 = 2.15$ is the same in all panels. Results are shown for two coupling constants $g = 0.1$ (dot–dashed curve) and $g = 0.4$ (dashed curve). In (a) and (c) the current is in the middle of the entrainment step, $I_0 = 1.97$ ($g = 0.1$) and $I_0 = 1.88$ ($g = 0.4$), whereas in (b) and (d) the current value is on the left-hand side of the step, $I_0 = 1.934$ ($g = 0.1$) and $I_0 = 1.77$ ($g = 0.4$). Other parameters are $p = 0.7$, $\phi = 0.8$ and $\sigma_\phi = 0.01$. Averages are over at least 40×10^3 cycles, after discarding the initial 200 cycles.

4. Discussion

The properties of the discharge of an ensemble of neurons can be measured in a number of different ways. One can pool the spike phases of all the neurons in all cycles together and calculate the variance σ_ψ^2 of the resulting distribution. This variance contains contributions from two cycle-related variances: σ_W^2, measuring the average width of the network discharge, and σ_B^2, measuring the jitter in the timing of the population discharge. Most studies concerned with collective enhancement of precision (CEP) focus primarily on σ_B. σ_W and σ_B are both biophysically relevant and here we have carefully studied their behaviour. We now briefly summarize our results for σ_W and σ_B.

An IAF neuron driven by a periodic inhibitory pulse train attains its highest precision (lowest value for σ_ψ) on $1 : m$ phase-locking steps. The 1:1 step has the largest width and is thus the most stable. In the presence of jitter σ_ϕ in the arrival times of the inhibitory pulses the highest precision is still obtained on the phase-locking step, but only in the middle, most stable part. There σ_ϕ and σ_ψ are linearly related, $\sigma_\psi = c_0 \sigma_\phi$. Skipping occurs close to the edges of the step and it always increases the output jitter. The spike trains of N independent (uncoupled)
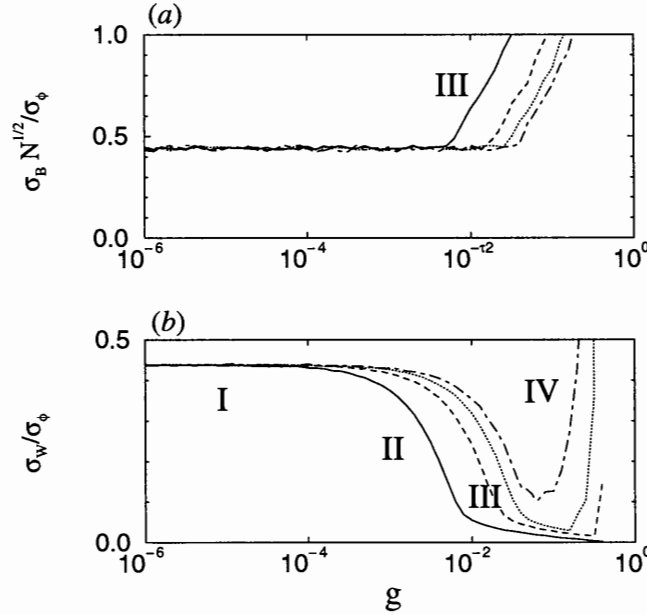
Figure 9. Crossover of precision from uncoupled to strongly coupled networks. (a) $\sigma_B\sqrt{N}/\sigma_\phi$ and (b) σ_W/σ_ϕ versus coupling strength g for $\sigma_\phi = 0.005$ (solid curves), 0.015 (dashed curves), 0.025 (dotted curves) and 0.035 (dot–dashed curves), with $p = 0.7$. The current I_0 is covaried with g to keep the fixed-point spike phase equal to $\psi = 0.383$. Roman numerals refer to regions of g defined in the text in section 3.5. Averages are over 5×10^3 cycles, after discarding the initial 100 cycles.

neurons pooled together yield a network discharge with $\sigma_B \approx \sigma_\psi/\sqrt{N}$, and $\sigma_W \approx \sigma_\psi$. The jitter σ_B in the network spike times therefore decreases quickly with increasing network size, but the width σ_W of the discharge in a given cycle remains unchanged.

For a coupled network the maximal precision is also attained in the middle of the phase-locking step. In a fully synchronized network we have by definition $\sigma_W \approx 0$ and $\sigma_B = c_g\sigma_{\mathrm{eff}}$. σ_{eff} is the variance in the distribution of $\Delta\phi_m^{\min}$, and it scales asymptotically as $\sigma_{\mathrm{eff}} \sim 1/\sqrt{\log N}$. We find numerically that this limit for σ_B is not reached, and that this expression should be interpreted as a lower bound. Therefore the CEP, $1/\sigma_B$, in the strongly coupled network is less than that of an uncoupled network.

At intermediate coupling strength there is a crossover in σ_W and σ_B from the uncoupled values to the strongly coupled values. The onset of the decrease in σ_W occurs at a lower coupling strength compared with the increase in σ_B. As a result there is an optimal value of g where σ_B is close to its optimal value (at $g = 0$), whereas σ_W is substantially reduced.

What are the functional consequences of these differences between coupled and uncoupled networks? It is desirable to have a low value for σ_W, since most neurons will spike more reliably when they are driven by a barrage of spikes that are close together in time compared with when there is a large dispersion. During transduction of network spike trains into a continuous electric signal, as occurs in the electric fish, a low σ_W would yield a much larger phasic-to-tonic ratio than a spike train with a higher value of σ_W. Here the limitations of the uncoupled network come to light: no matter how many neurons there are in the network σ_W will stay the same and equal to the original jitter in a single neuron. In a coupled network one can find values for N and g that satisfy arbitrary requirements on σ_W and σ_B.

In this study we have investigated how precision increases with network size N using a simple neural model. The model lacks features that are present in physiological systems, such as a time scale for EPSPs and IPSPs, and it produces zero-width action potentials. Furthermore, functionally important synaptic effects such as facilitation and depression were not taken into account [15, 16]. Despite its simplicity the model produces phase-locking steps in the firing rate. Phase locking of neuronal discharge to a periodic injected current, periodic presynaptic spike trains and even synchronized network discharge are ubiquitous in the nervous system. Phase locking has been studied theoretically in IAF neurons [17–20], Fitzhugh–Nagumo models [21] and Hodgkin–Huxley-based models [22]. Recently, it was shown that entrainment or phase locking can lead to a precision resonance [22–24]. Here we investigated how precision resonance in combination with recurrent excitation influences the CEP. We also specifically address the effect of jitter in the input spike train. The main advantage of the present approach is that analytical estimates for large-N networks can be obtained and tested using efficient simulations. However, it is important to determine how our estimates carry over to more biophysically accurate models, which will be the subject of future research.

Acknowledgments

Appendix

The variance of the distribution $P_{\min}$ determines the output jitter of the strongly coupled network. Here we determine the asymptotics of the variance for very large networks to complement the numerical results for small to large networks described in the main body of the text. In the following we determine $P_{\min}$ exactly and then proceed to make a number of approximations to find the first and second moments as a function of network size N.

First we calculate the distribution of $\Delta\phi_m^{\min}$, the minimum value of $\Delta\phi_m^n$ in a given cycle m, as a function of the network size (for simplicity we use the notation $x = \Delta\phi_m^{\min}$ and $\sigma = \sigma_\phi$). The distribution of the minimum of N independent, identically distributed variables with probability distribution function $P(x)$ and cumulative probability distribution $\delta(x)$ reads [25]

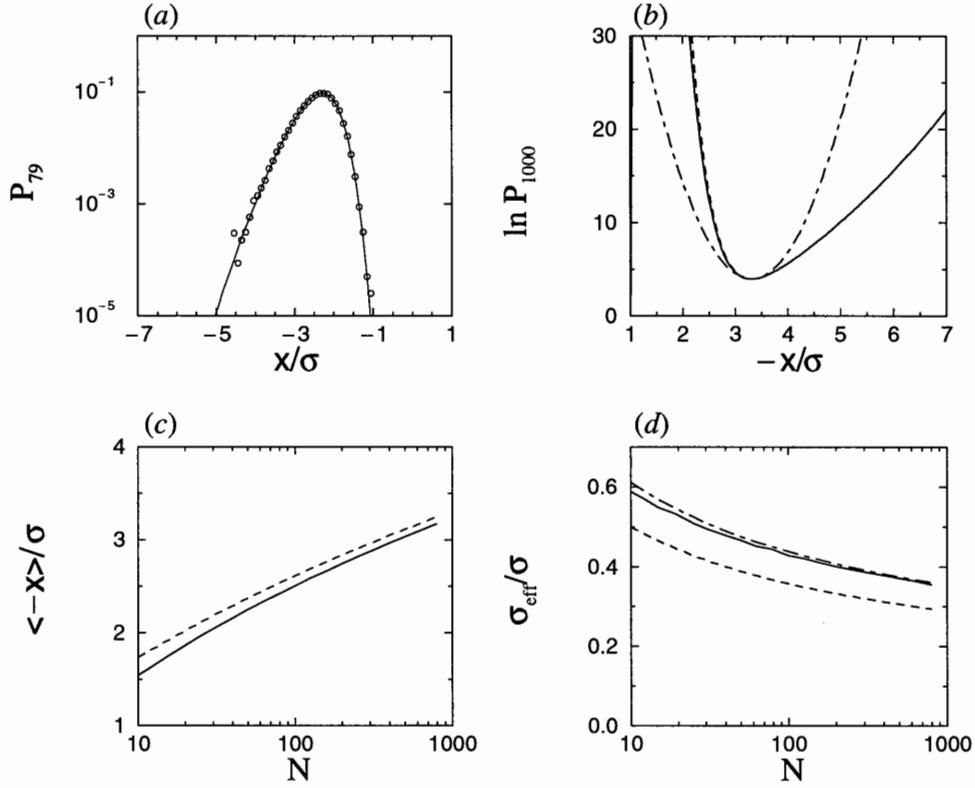$$P_{\min}(x, N) = N P(x)(1 - \delta(x))^{N-1} \equiv e^{-F}, \tag{27}$$

where

$$P(x) = \frac{1}{\sqrt{2\pi\sigma^2}} \exp\left(-\frac{x^2}{2\sigma^2}\right), \tag{28}$$

is the distribution of the original $x = \Delta\phi_m^n$, and

$$1 - \delta(x) = \int_x^\infty P(y)\,dy = \frac{1}{2} - \frac{1}{2}\mathrm{erfc}\left(\frac{x}{\sqrt{2}\sigma}\right). \tag{29}$$

There is excellent agreement between $P_{\min}$ determined using numerical simulations and the analytical expression equation (27) (figure A.1(a)). We expand δ asymptotically in $1/x$

Figure A.1. Comparison of simulations to analytical results. (a) Distribution of the minimum x obtained from simulations (open circles), and the result of equation (27) (solid curve) for $N = 79$. (b) Exponent of equation (27) (continuous curve) compared with the asymptotic expansion equation (31) (dashed curve), and the saddle point expansion equation (35) (dot–dashed curve). (c) Average obtained from simulations (continuous curve) compared with the saddle point position x_0 (equation (36), dashed curve). (d) Standard deviation from simulations (continuous curve) compared with equation (36) (dashed curve). The dot–dashed curve is the dashed curve multiplied by $\sqrt{\frac{3}{2}}$. Averages over 80×10^3 cycles, after discarding the initial 2×10^3 cycles.

for large *negative x*,

$$\delta(x) \approx -\frac{1}{\sqrt{2\pi}}\frac{\sigma}{x}e^{-\frac{x^2}{2\sigma^2}}\left(1 - \frac{\sigma^2}{x^2}\right). \tag{30}$$

Then, using the approximation $\log 1 - \delta \approx -\delta$, we obtain

$$F(x) \approx \frac{x^2}{2\sigma^2} - (N-1)\frac{1}{\sqrt{2\pi}}\frac{\sigma}{x}e^{-\frac{x^2}{2\sigma^2}}\left(1 - \frac{\sigma^2}{x^2}\right). \tag{31}$$

In figure A.1(b) the result of equation (31) to the exact result (equation (27)). We find excellent agreement for $N > 1000$ and $-x/\sigma > 2$. We further approximate the distribution using the saddle point expansion. The first derivative of F is (up to second order in $\frac{\sigma}{x}$)

$$F'(x) = \frac{x}{\sigma^2} + \frac{N-1}{\sigma\sqrt{2\pi}}e^{-\frac{x^2}{2\sigma^2}}. \tag{32}$$

The minimum of F is located at x_0 given by $F'(x_0) = 0$,

$$\frac{x_0}{\sigma} = -\frac{N-1}{\sqrt{2\pi}}e^{-\frac{x_0^2}{2\sigma^2}}. \tag{33}$$

The value of the second derivative at x_0 is

$$F''(x_0) = \frac{1}{\sigma^2} - \frac{N-1}{\sqrt{2\pi}}\frac{x_0}{\sigma^3}e^{-\frac{x_0^2}{2\sigma^2}} = \frac{1}{\sigma^2}\left(1 + \frac{x_0^2}{\sigma^2}\right). \tag{34}$$

Using the above results we get for the saddle-point expansion

$$F_{\text{saddle}} = F(x_0) + \tfrac{1}{2}F''(x_0)(x - x_0)^2. \tag{35}$$

In figure A.1(b) we compare this expression to equations (27) and (31). Equation (35) only yields a good approximation for x values close to x_0. The saddle point expansion defines a Gaussian probability distribution with mean x_0 and variance $\sigma_{\text{eff}}^2 = 1/F''(x_0)$. For exponentially large N, $\ln N \gg 1$, we obtain

$$\frac{x_0}{\sigma} \sim -\sqrt{2\ln(N-1)},$$

$$\frac{\sigma_{\text{eff}}^2}{\sigma^2} \sim \frac{1}{1 + 2\ln(N-1)}. \tag{36}$$

We have compared these asymptotic estimates to the mean and variance determined by numerical integration of equation (27). The exact results only slowly converge to their asymptotic estimates. This indicates that the asymptotics are only valid for large $N > 1000$.

References

[1] Moortgat K T, Keller C H, Bullock T H and Sejnowski T J 1998 Submicrosecond pacemaker precision is behaviorally modulated: the gymnotiform electromotor pathway *Proc. Natl Acad. Sci. USA* **95** 4684–9
[2] Moortgat K T, Bullock T H and Sejnowski T J 2000 Precision of the pacemaker nucleus in a weakly electric fish: network versus cellular influences *J. Neurophysiol.* **83** 971–83
[3] Moortgat K T, Bullock T H and Sejnowski T J 2000 Gap junction effects on precision and frequency of a model pacemaker network *J. Neurophysiol.* **83** 984–97
[4] Knight B W 1972 Dynamics of encoding in a population of neurons *J. Gen. Physiol.* **59** 734–66
[5] Knight B W 1972 The relationship between the firing rate of a single neuron and the level of activity in a population of neurons. Experimental evidence for resonant enhancement in the population response *J. Gen. Physiol.* **59** 767–78
[6] Needleman D J, Tiesinga P H E and Sejnowski T J 2001 Collective enhancement of precision in networks of coupled oscillators *Physica* D at press
[7] Mainen Z F and Sejnowski T J 1995 Reliability of spike timing in neocortical neurons *Science* **268** 1503–6
[8] Reichl L E 1998 *A Modern Course in Statistical Physics* 2nd edn (New York: Wiley) p 199
[9] Press W H, Teukolsky S A, Vetterling W T and Flannery B P 1992 *Numerical Recipes* 2nd edn (Cambridge: Cambridge University Press)
[10] Hansel D, Mato G, Meunier C and Neltner L 1998 On numerical simulations of integrate-and-fire neural networks *Neural Comput.* **10** 467–83
[11] van Vreeswijk C, Abbott L F and Ermentrout G B 1994 When inhibition not excitation synchronizes neural firing *J. Comput. Neurosci.* **1** 313–22
[12] Terman D and Wang D L 1995 Global competition and local cooperation in a network of neural oscillators *Physica* D **81** 148–76
[13] Hansel D, Mato G and Meunier C 1995 Synchrony in excitatory neural networks *Neural Comput.* **7** 307–37
[14] Gerstner W, van Hemmen J L and Cowan J 1996 What matters in neuronal locking? *Neural Comput.* **8** 1653–76
[15] Abbott L F, Varela J A, Sen K and Nelson S B 1997 Synaptic depression and cortical gain control *Science* **275** 220–4
[16] Markram H, Wang Y and Tsodyks M 1998 Differential signaling via the same axon of neocortical pyramidal neurons *Proc. Natl Acad. Sci. USA* **95** 5323–8

[17] Keener J, Hoppensteadt F and Rinzel J 1981 Integrate-and-fire models of nerve membrane response to oscillatory input *SIAM J. Appl. Math.* **41** 503–17

[18] Tateno T 1998 Characterization of stochastic bifurcations in a simple biological oscillator *J. Stat. Phys.* **92** 675–705

[19] Coombes S and Bressloff P C 1999 Mode locking and Arnold tongues in integrate-and-fire neural oscillators *Phys. Rev.* E **60** 2086–96

[20] Tateno T and Jimbo Y 2000 Stochastic mode-locking for a noisy integrate-and-fire oscillator *Phys. Lett.* A **271** 227–36

[21] Longtin A and Chialvo D R 1998 Stochastic and deterministic resonances for excitable systems *Phys. Rev. Lett.* **81** 4012–5

[22] Tiesinga P H E and José, J V 2000 Robust gamma oscillations in networks of inhibitory hippocampal interneurons *Network* **11** 1–23

[23] Hunter J D, Milton J G, Thomas P J and Cowan J D 1998 Resonance effect for neural spike time reliability *J. Neurophysiol.* **80** 1427–38

[24] Tiesinga P H E, Fellous J-M, José J V and Sejnowski T J 2001 Optimal information transfer in synchronized neocortical neurons *Neurocomputing* **38–40** 397–402

[25] Larsen R J and Marx M L 1986 *An Introduction to Mathematical Statistics and its Applications* 2nd edn (Englewood Cliffs, NJ: Prentice-Hall) p 146